Journal of Alloys and Compounds 509 (2011) 1187–1191

Contents lists available at ScienceDirect

Journal of Alloys and Compounds

journal homepage: www.elsevier.com/locate/jallcom

Effects of SiC volume fraction and aluminum particulate size on interfacial reactions in SiC nanoparticulate reinforced aluminum matrix composites

Bowen Xiong[a,b,*], Zhifeng Xu[a,b], Qingsong Yan[a,b], Baiping Lu[a], Changchun Cai[a,b]

[a] National Defence Key Discipline Laboratory of Light Alloy Processing Science and Technology, Nanchang Hangkong University, Nanchang 330063, PR China
[b] School of Aeronautical Manufacturing Engineering, Nanchang Hangkong University, Nanchang 330063, PR China

ARTICLE INFO

Article history:
Received 1 September 2010
Received in revised form
19 September 2010
Accepted 26 September 2010
Available online 30 October 2010

Keywords:
Metal matrix composites
Microstructure
Interfacial reaction
Nanoparticulate

ABSTRACT

The SiC nanoparticulate reinforced Al–3.0 wt.% Mg composites were fabricated by combining pressureless infiltration with ball-milling and cold-pressing technology at 700 °C for 2 h. The effects of SiC nanoparticulate volume fractions (6%, 10% and 14%) and Al particulate sizes (38 μm and 74 μm) on interfacial reactions were investigated by SEM, TEM and X-ray diffraction. The results show that the MgO at the interface between SiC nanoparticulate and molten Al can provide a barrier for the diffusion of Si, C and Al. Using Al particulate (74 μm) as raw material, the Al_4C_3 phase was not found in the composites containing 6 vol.% and 10 vol.% SiC, but presented in the composites containing 14 vol.% SiC. When SiC content up to 14 vol.%, the products of MgO around SiC nanoparticulate are not enough to provide effective protection from the reaction between SiC and molten Al, therefore the diffusion of Si, C and Al can take place to produce Al_4C_3 and Si phases. Using 38 μm Al particulate as raw material, the fine Al particulate possesses the high reaction activity and can easily be embedded into the gap among the big Mg particulate segregated at the interface, resulting in the appearance of exposure surface of SiCp to the Al and the forming of diffusion channels for the atomics C, Si and Al. So, the formations of Al_4C_3 and Si phases were occurred.

1. Introduction

SiC particulate reinforced Al-based metal matrix composites (MMCs) have been considered as excellent candidates to be applied as structural material in the aerospace and automobile industry [1]. Compared with the unreinforced matrix alloy, Al-based MMCs have attractive physical and mechanical properties, such as high strength, high hardness and superior wear resistance. It has been reported that higher mechanical strength of particulate reinforced metal matrix composites can be achieved by decreasing the reinforcement particulate size [2–5]. Nanoparticulate as the reinforcement can significantly increase the matrix mechanical strength by more effectively promoting particle hardening mechanisms than micron size particulate [6]. However, the possible chemical interfacial reactions between the fine SiC particulate (especially nanoparticulate) and Al matrix play a crucial role in determining the mechanical property of Al matrix composites. The very high ratio of surface to volume of SiC nanoparticulate induces the higher interfacial reaction activity than micron size particulates. In order to obtain excellent mechanical properties, it is indispensable to form desired interfaces.

Some interfacial reactions in metal matrix composites can effectively improve the mechanical properties of composites by enhancing of the wettability between particulates and molten metal [7–10], but some of interfacial reactions also cause the degradation of mechanical properties due to the formation of brittle and unstable phases (e.g., Al_4C_3). The reaction between molten Al and SiC particulates in the temperature range from 675 °C to 900 °C has been widely investigated, producing Al_4C_3 and silicon according to the following reaction equation [11–14]:

$$4Al + 3SiC \rightarrow Al_4C_3 + 3Si \quad (1)$$

However, the existing investigations on the interfacial reactions in metal matrix composites are mainly related to three topics for controlling the interfacial reactions: (1) control of matrix composition, such as SiC/Al composites. The above interfacial reactions can be suppressed to hinder the formation of Al_4C_3 phase by adding Si element into Al matrix alloy [15–17]. (2) Selection of process parameters, for example, fabrication temperature and holding time, etc. [18,19]. (3) Surface modification of reinforcement, for instance, the coating or oxidation of SiC particulate [20]. Thus, little attention has been paid to the effects of SiC nanoparticulate volume fraction and aluminum matrix particulate size on interfacial reactions in SiC nanoparticulate reinforced aluminum matrix composites. And from the available literatures, the investigations about these effects on interfacial reactions are limited to providing the

* Corresponding author at: School of Aeronautical Manufacturing Engineering, Nanchang Hangkong University, Nanchang 330063, PR China.
E-mail address: bowenxiong@163.com (B. Xiong).

0925-8388/$ – see front matter.
doi:10.1016/j.jallcom.2010.09.171

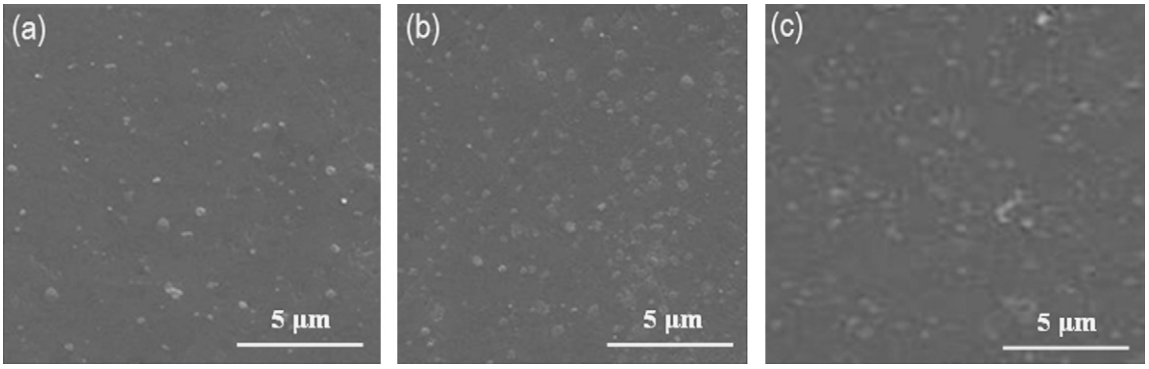

Fig. 1. The distribution of SiC nanoparticulates reinforcement in the B1, B2 and B3 composites.

desired information and completed apprehension. In present investigation, the pressureless infiltration combining with ball milling and cold pressing technology was employed to fabricate the composites [21]. The objectives of the present study are to investigate on the effects of SiC volume fraction and aluminum matrix particulate size on interfacial reactions between SiC nanoparticulate and molten aluminum, and to achieve the significant information for controlling the interfacial reactions.

2. Experimental procedure

The Al (the mean size approximate to 38 μm and 74 μm) with purity of 99.5 wt.% and 3 wt.% Mg (approximately 74 μm) with purity of 99.6 wt.% were used as matrix and reinforced with 6 vol.%, 10 vol.% and 14 vol.% SiC (40 nm) respectively. The composites designations are summarized in Table 1. High-energy ball milling has been widely utilized for mixing SiC nanoparticulate and Al particulate. High-energy ball milling was performed in a planetary ball milling using 200 hardened stainless steel balls of 4 g each. The ratio of ball to particulate weight was 4:1. The rotational speed was controlled at 450 rpm. These particulates were dry mixed for 10 h in a high purity of 99.99% argon atmosphere to avoid element oxidation. The mixed particulates were compressed to prepare the preform with dimensions of 40 mm × 40 mm × 80 mm by the cold pressing technology under a pressure of 50 GPa.

The identical composition with matrix material was melted in a graphite crucible kept in an electric resistance furnace, using a flux mixture of salts (KCl + NaCl) to decrease oxidation of material by excluding oxygen and provide a protective atmosphere inside the electric resistance furnace. When the temperature of furnace was raised to 700 °C and held for 20 min, the preforms for pressureless infiltration were put into and suspended inside the molten material for 2 h, and subsequently the composites were cooled inside furnace.

The microstructural characterization specimens were prepared by grinding paper from 320 to 1200 grit and metallographically polished with 1 μm alumina, and subsequently ultrasonically cleaned and etched using a reagent comprising 5 ml HF and 95 ml distilled water. The microstructures were examined using a MeF-3 optical microscope and a JSMT-200 scanning electron microscope. D/MAX-IIIB X-ray diffraction was performed on the bulk specimens for identification of phases. The interface between the Al matrix and SiC nanoparticulate was investigated using JEM200 transmission electron microscope.

3. Results and discussion

The distribution of SiC nanoparticulates reinforcement in the B1, B2 and B3 composites was investigated by optical microscope and presented in Fig. 1. The SEM study of composite samples reveals uniform distribution of SiC nanoparticulates in the Al–3% Mg matrix. Only C3 composite sample shows the agglomeration of SiC nanoparticulates in some region. The desirable uniform distribution of SiC nanoparticulates indicates that the high-energy ball milling process was optimized for the distribution of SiC nanoparticulates. The appearance of SiC agglomeration in the C3 composite may be owing to the finer size of Al particulate and high volume fraction of SiC nanoparticulate. The higher volume fraction and large surface to volume ratio of fine particulate in C3 composite induce a hard task to uniform distribution and dispersion of reinforcement particles throughout the metal matrix [22]. Therefore, the agglomeration of SiC nanoparticulates takes place in C3 composite. The agglomeration of SiC nanoparticulates in the C3 composite are shown in Fig. 2. The XRD patterns of the B1, B2 and B3 composites are presented in Fig. 3, and the XRD patterns of the C1, C2 and C3 composites are shown in Fig. 4. Individual phases were identified by matching the characteristic XRD peaks against JCPDS data. It is obvious from Fig. 3 that the peaks of Mg_2Si, Al_4C_3, MgO and Si were detected in B3 composite, whereas the peaks of Al_4C_3 and Si were not detected in B1 and B2 composites, and with the increasing of SiC volume fraction, the intensity of Mg_2Si peaks increases but the intensity of MgO peaks reduces. It is evident from Fig. 4 that the peaks of Mg_2Si, Al_4C_3, MgO and Si were found in the three composites. Although the B1 and C1 (similarly B2 and C2) composites have the same SiC nanoparticulate volume fraction, the reaction products are obviously different. These phenomena show that the interfacial reactions can take place

Table 1
Composites designation.

NanoSiC (vol.%)	Al particulate size (μm)	Designation
6	74 μm	B1
10		B2
14		B3
6	38 μm	C1
10		C2
14		C3

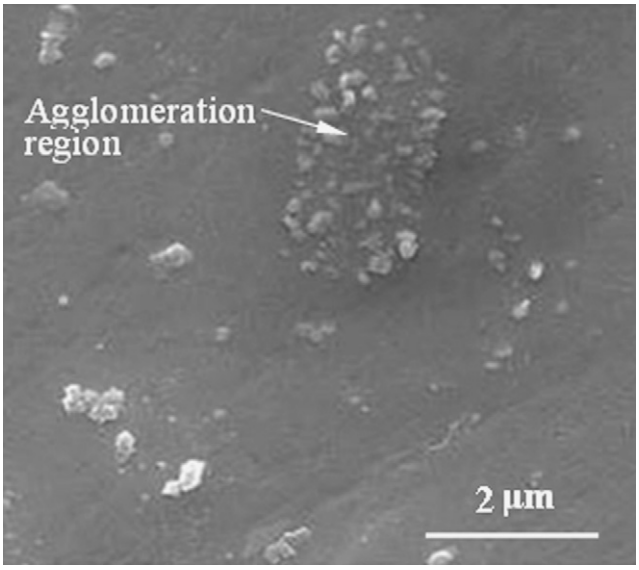

Fig. 2. The agglomeration of SiC nanoparticulates in the C3 composite.

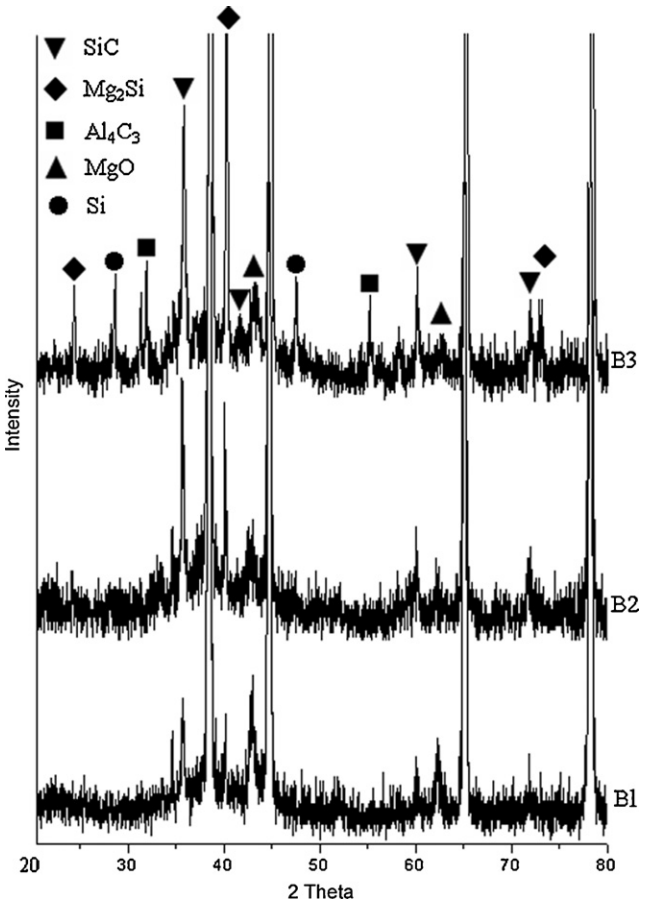

Fig. 3. The XRD patterns of the B1, B2 and B3 composites.

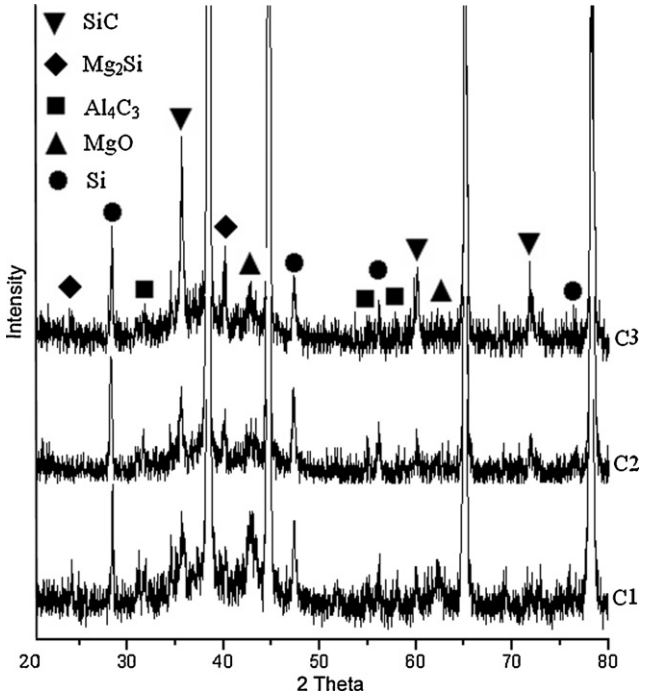

Fig. 4. The XRD patterns of the C1, C2 and C3 composites.

in composites, and the SiC nanoparticulate volume fraction and aluminum matrix particulate size affect the interfacial reactions. In order to further analyze the interfacial reactions, the interfacial regions of the as-cast composites were observed by TEM and the phases were determined by selected area diffraction analysis. The interfacial micrographs of B1 composite are identical with the B2 composite from the observation, whereas, completely different from that of the other composites, which indicate similar interfacial micrographs. The typical interfacial micrographs of composites are shown in Fig. 5(a) and (b). The SAD patterns were given in Fig. 5(c)–(e). The Mg_2Si and MgO phases were detected in B1 and B2 composites and Al_4C_3 and Si phases were absented (Fig. 5(a)). Whereas, the Al_4C_3 and Si phases were presented in other composites (Fig. 5(b)). Therefore, the interfacial reaction mechanisms of B1 and B2 composite are obviously different from that of the other composites.

The presence of Al_4C_3, MgO, Mg_2Si, $MgAl_2O_4$, and Si phases formed by interfacial chemical reaction among Al, Mg and SiC has been reported, according to Eq. (1) and following equations:

$$4Mg + SiO_2 \rightarrow 2MgO + Mg_2Si \quad (2)$$

$$2Al + 5Mg + 2SiO_2 \rightarrow MgAl_2O_4 + 2Mg_2Si \quad (3)$$

$$2Mg + Si \rightarrow Mg_2Si \quad (4)$$

$$4Al + 3SiO_2 \rightarrow 2Al_2O_3 + 3Si \quad (5)$$

Due to the SiC nanoparticulate having the higher surface energy and activity than micron particulates is prone to absorb the gas, such as O_2. Therefore, SiC nanoparticulate can be oxidized to form SiO_2 product during the pressureless infiltration at 700 °C for 2 h. Furthermore, the reaction kinetics and tendency of Mg and SiO_2 are several times stronger than that of Al and SiO_2 at 680–800 °C [23,24], thus, Mg is more prone to react with the surface oxides SiO_2 than Al to form the Mg_2Si and MgO phases. As Mg element is added, the $MgAl_2O_4$ and Al_2O_3 phases are possible to form individually and in combination, but there has been no evidence of $MgAl_2O_4$ and Al_2O_3 phases in the present study from XRD patterns and Fig. 5.

During the fabrication of Al/SiC composite by isothermal infiltration technology, the SiC particulate was generally decomposed in molten Al and forms Si and C elements. With the decomposing of SiC at a given temperature, the C thermodynamic equilibrium concentration has been reached firstly, because of the low solubility of C in molten Al. In order to keep the C thermodynamic equilibrium concentration, the C will react with Al to form Al_4C_3 phase according to Eq. (1) until the Si content up to the thermodynamic equilibrium concentration. Therefore, with the increasing of SiC volume fraction, the Si content will increase from Eq. (1). Because of increasing of Si content, the content of Mg_2Si phase is increases from Eq. (4). As Mg content is constant and Mg_2Si phase is increases, the decreasing of MgO content can be found. Therefore, the phenomena that the intensity of Mg_2Si peaks increases and that of MgO peaks reduces with increasing of SiC volume fraction was detected from XRD patterns. Moreover, when Mg is added, the segregation of Mg at the SiC/Al interface was frequently detected [25–27]. The segregation of Mg at the interface will react with SiO_2 or the O_2 trapped during the fabrication process to form MgO. In Fig. 5(a), the much MgO phase around the SiC was found, and the formation of MgO can enhance the wettability and provide a barrier for the diffusion of Si, C and Al. Thus, the Si and C can rapidly reach their thermodynamic equilibrium concentration around the SiCp region, and the decomposing of SiCp is suppressed. The extent of reaction between molten Al and SiCp is obviously decreased.

Al particulate (74 μm) was used in B1, B2 and B3 composites. The B1 and B2 composites which do not present the reaction products Al_4C_3 and Si phases from Fig. 3, whereas the content of SiCp up to 14 vol.% obviously leads to the formation of Al_4C_3 and Si in

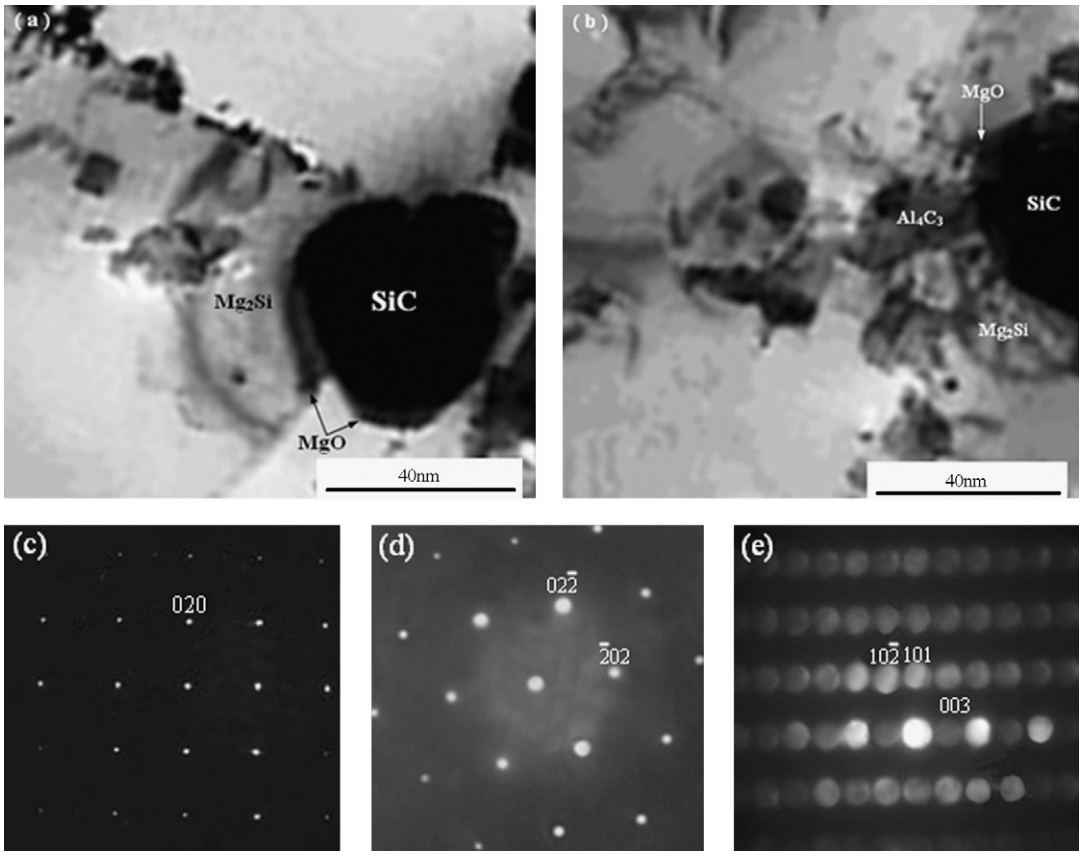

Fig. 5. The typical interfacial micrographs of composites: (a) TEM image of interface in B2 composite, (b) TEM image of interface in B3 composite, (c) SAD pattern of Mg_2Si, (d) SAD pattern of MgO, and (e) SAD pattern of Al_4C_3.

B3 composite. This phenomenon may be explained by the fact that the formation of MgO at the interface between SiC nanoparticulates and molten Al can effectively reduce the contacted surface of the SiC nanoparticulates to the molten Al and provide a barrier for the diffusion of Si, C and Al, resulting in the Si and C elements around SiCp can reach quickly thermodynamic equilibrium concentration for suppressing the decomposing of SiCp. when Mg content is 3 wt.% and SiC content is 6 vol.% and 10 vol.%, the products of MgO around SiC nanoparticulates are enough to form a diffusion barrier for reaction between SiCp and molten Al, whereas Mg content is constant but SiC content up to 14 vol.% in the B3 composite, the products of MgO around SiC nanoparticulates are not enough to form effective protection from the reaction between SiCp and molten Al, and little MgO phase around the SiC was found in Fig. 5(b), therefore the diffusion of Si, C and Al can take place and produce Al_4C_3 and Si phases in the B3 composite (Fig. 5(b)).

Al particulate with the 38 μm size was used in the C1, C2 and C3 composites. Although the B1 and C1 (similarly B2 and C2) composites have the same SiC nanoparticulate volume fraction, compared the XRD patterns of B1with C1 and B2 with C2, respectively, the peaks of Al_4C_3 and Si were found in the C1 and C2 composites but not found in the B1 and B2 composites. This investigation result may be explained by the reason that the Al particulate used in the C1 and C2 composite is finer than used in B1 and B2 composites. The fine Al particulate (38 μm) possesses the higher reaction activity than that of 74 μm Al particulate, on the other hand, when the 74 μm Mg particulates segregate at the interface between SiCp and Al, the fine Al particulate can be embedded into the gap among the big Mg particulate, resulting in the forming of the exposure surface of SiCp to the Al and the diffusion channel for the atomics C, Si and Al. Consequently, the formation of Al_4C_3 and Si phases occurred following the chemical reaction between SiC and liquid Al (Eq. (1)).

4. Conclusions

The SiC nanoparticulate reinforced Al matrix composites was fabricated by combining pressureless infiltration with ball-milling and cold-pressing technology at 700 °C for 2 h. The effects of SiC volume fraction and Al matrix particulate size on interfacial reactions between SiC nanoparticulate and the molten Al were investigated. The results obtained are summarized as follows:

When Mg was added to the Al matrix, the formations of MgO at the interface between SiC nanoparticulate and molten Al were found, which can enhance the wettability and provide a barrier for the diffusion of Si, C and Al.

Using Al particulate (74 μm) as raw material, the Al_4C_3 phase was not found in the composites containing SiC nanoparticulate 6 vol.% and 10 vol.% respectively, but present in the composites containing SiC nanoparticulate 14 vol.%. When SiC content up to 14 vol.%, the products of MgO around SiC nanoparticulate are not enough to form effective protection from the reaction between SiCp and molten Al, therefore the diffusion of Si, C and Al can take place and produce Al_4C_3 and Si phases.

Using 38 μm Al particulate as raw material, the finer Al particulate possesses the high reaction activity and can easily be embedded into the gap among the big Mg particulate, which segregate at the interface between SiCp and Al, resulting in the appearance of exposure surface of SiCp to the Al and diffusion channels for the atomics C, Si and Al. So, the formation of Al_4C_3 and Si phases was detected.

Acknowledgements

This research was financially supported by Science and Technology Fund of Jiangxi Provincial Department of China (Grant Number: GJJ08199), and Open Fund of Aeronautical Science and Technology

Key Lab. of Aeronautical Materials Processing, Nanchang Hangkong University of China (Grant Number: ZK200901002).

References

[1] O. Tamer, K. Erol, Ç. Orhan, J. Mater. Process. Technol. 198 (2008) 220–225.
[2] Y. Yang, J. Lan, X. Li, Mater. Sci. Eng. A 380 (2004) 378–383.
[3] S.F. Hassan, M. Gupta, Mater. Sci. Eng. A 392 (2005) 163–168.
[4] L. Lu, M.O. Lai, W. Liang, Compos. Sci. Technol. 64 (2004) 2009–2014.
[5] Z.Y. Ma, S.C. Tong, Y.L. Li, Compos. Sci. Technol. 59 (1999) 263–270.
[6] G. Cao, H. Konishi, X. Li, Mater. Sci. Eng. A 392 (2007) 163–168.
[7] F. Delannay, L. Froyen, A. Deruyttere, J. Mater. Sci. 22 (1987) 1–16.
[8] H. Ribes, M. Suery, G. Esperance, J.G. Legoux, Metall. Trans. A 21 (1990) 2489–2495.
[9] M.Y. Gu, Z. Mei, Y.P. Jin, Z.G. Wu, Scripta Mater. 40 (1999) 985–989.
[10] S.G. Warrier, R.Y. Lin, J. Mater. Sci. 28 (1993) 760–766.
[11] D.J. Lloyd, H. Lagace, A. McLeod, P.L. Morris, Mater. Sci. Eng. A 107 (1989) 73–86.
[12] D.J. Lloyd, H. Jin, Metall. Trans. A 19A (1988) 3017–3019.
[13] C.A. Handwerker, J.W. Cahn, J.R. Manning, Mater. Sci. Eng. A 126 (1990) 173–180.
[14] J.C. Vilala, P. Fortier, J. Bouix, J. Mater. Sci. 25 (1990) 1842–1850.
[15] D.J. Lloyd, Compos. Sci. Technol. 35 (1989) 159–179.
[16] J.-C. Lee, J.-Y. Byun, S.-B. Park, H.-I. Lee, Acta Mater. 46 (1998) 1771–1780.
[17] R.Y. Lin, Interface Evolution in Aluminum Matrix Composites During Fabrication. Key Engineering Materials, vol. 104–107, Trans Tech Publications, Switzerland, 1995, pp. 507–522.
[18] T.X. Fan, D. Zhang, Z.L. Shi, R.J. Wu, J. Mater. Sci. 34 (1999) 5175–5181.
[19] J.C. Lee, G.H. Kim, H.I. Lee, Mater. Sci. Technol. 13 (1997) 182–188.
[20] Z.L. Shi, O. Shojiro, H. Masaki, M.Y. Gu, R.J. Wu, J. Mater. Sci. 36 (2001) 2441–2449.
[21] B.W. Xiong, Z.F. Xu, Q.S. Yan, C.C. Cai, Y.H. Zheng, B.P. Lu, J. Alloy Compd. 497 (2010) L1–L4.
[22] D.L. Zhang, J. Liang, J. Wu, Mater. Sci. Eng. A 375–377 (2004) 911–916.
[23] T. Stepenson, Y. Le Petitcorps, J.M. Quenisset, Mater. Sci. Eng. A 135 (1991) 101–112.
[24] W.M. Zhang, G. L'espérance, M. Suéry, Metall. Trans. A 26 (1995) 2637–2649.
[25] H. Ribes, R. Da Sliva, M. Suery, T. Bretheau, Mater. Sci. Technol. 6 (1990) 621–628.
[26] M. Strangewood, C.A. Hippley, J.J. Lewandowski, Scripta Metall. 24 (1990) 1483–1492.
[27] M. Fishkis, J. Mater. Sci. 26 (1991) 2651–2661.